DEFECTS IN LIQUID CRYSTALS: SURFACE AND INTERFACIAL ANCHORING EFFECTS

O.D. Lavrentovich
Liquid Crystal Institute and Chemical Physics Interdisciplinary Program, Kent State University, Kent, OH 44242, U.S.A.

Abstract This review discusses static properties of topological defects, such as line defects-disclinations and dislocations, point defects - hedgehogs (monopoles) and boojums; focal conic domains and tilt grain boundaries in basic types of liquid crystals: uniaxial and biaxial nematics, cholesterics and smectics. We present the most popular experimental techniques to study defects in soft matter, namely, polarizing microscopy and fluorescence confocal polarizing microscopy. The role of bounding surfaces and the so-called surface anchoring that lifts the degeneracy of the order parameter in stability of defects is discussed. Because of the surface anchoring, the equilibrium state of a bounded liquid crystal might contain topological defects. For example, nematic bubbles nucleating during the first-order phase transition from the isotropic melt, might contain point defects (hedgehogs and boojums) and disclination loops when their size is larger than the anchoring extrapolation length defined by the ratio of the Frank elastic constant of the director curvature and the (polar) anchoring coefficient. Depending on the strength of surface anchoring, an edge dislocation might be expelled from the system with 1D positional order or be stabilized in the bulk. Furthermore, focal conic domains play the role of "surface anchoring facets" by providing the necessary orientation of the liquid crystal director at the smectic boundary.

1. Introduction

Liquid crystals are endowed with continuous symmetries and physical prevalence of correlations of orientation over correlations of position and thus show rich and complex variety of topological defects. Defects in liquid crystals are of various dimensionalities, not only line defects, but also points, walls, and "configurations" (walls, topological solitons). In this review, we consider basic properties (mainly static) of defects in the simplest types of liquid crystals, nematics and smectics, mostly in relationship to the experimental studies and effects that the bounding surfaces have on defects. The experimental techniques of regular polarizing microscopy and more recent fluorescent confocal

H. Arodz et al. (eds.), Patterns of Symmetry Breaking, 161–195.

polarizing microscopy are outlined in order to help those who would like to explore the word of liquid crystal defects experimentally. The discussion follows the textbook on soft matter physics [1] with an addition of some recent results. An interested reader is also referred to general reviews on liquid crystals [2–4] and defects in them [5, 6, 11, 12].

Liquid crystals are made of strongly anisometric molecules, either elongated (calamitic molecules) or disk-like (discotic molecules). As a rule, the central part of mesogenic molecules is rigid (phenyl groups) and the outer part flexible (aliphatic chains). This double character explains the existence of steric interactions (between rod-like or disk-like cores of the molecules) yielding orientational order and the fluidity of the liquid crystalline phases. Upon heating, many substances made of strongly anisometric molecules, exhibit the following phase sequence: solid crystal with a long–range orientational and positional order⇔liquid crystal (or mesophase) with a long-range orientational order and partial or no positional order ⇔isotropic fluid with no orientational nor positional long-range order. There are four basic types of liquid crystalline phases, classified according to the dimensionality of the translational correlations of building units: nematic (no translational correlations), smectic (1D correlations), columnar (2D correlations), and various 3D-correlated structures, such as cubic phases.

Uniaxial nematics, noted UN, are optically uniaxial fluid phases. The unit vector along the optic axis is called the director $\mathbf{n}$, $\mathbf{n}^2 = 1$; it indicates the average orientation of the molecular axes. Even when the building units are polar, molecular flip-flops and head-to-head overlapping establish centrosymmetric (average) arrangement in the nematic bulk. Thus, $\mathbf{n}$ and $-\mathbf{n}$ are equivalent notations. In biaxial nematics (BN), the symmetry point group is one of a prism. A BN phase is characterized by three directors, $\mathbf{n}$, $\mathbf{l}$, and $\mathbf{m} = \mathbf{n} \times \mathbf{l}$, such that $\mathbf{n} = -\mathbf{n}$, $\mathbf{l} = -\mathbf{l}$, and $\mathbf{m} = -\mathbf{m}$. Both UN and BN phases are fluid: the centers of gravity of the molecules are not correlated.

When the building block (molecule or aggregate) is chiral, i.e., not equal to its mirror image, the nematic phase might show helicoidal structure. It is then called a cholesteric phase N*. A rotation by an angle α about the cholesteric axis is equivalent to a translation $p\alpha/2\pi$; p is the pitch of the cholesteric helix, and it is twice the periodicity along the axis. An N* phase can be characterized by three directors: $\mathbf{n}$ along the local molecular axes, $\mathbf{t}$ along the axis of helicity (which is also the optic axis if the pitch is much smaller than the light wavelength), and $\mathbf{m} = \mathbf{n} \times \mathbf{t}$. Both BN and N* phases are liquid phases (no correlations in molecular positions).

Smectics are layered phases with quasi-long-range 1D translational order of centers of molecules in a direction normal to the layers. This positional order is not exactly the long-range order as in normal 3D crystals: As shown by Landau and Peierls, the fluctuative displacements of layers in 1D lattice diverge

logarithmically with the linear size of the sample. However, the effect is noticeable only on scales of 1 km and more [1]; typical samples are thinner: e.g., liquid crystal displays use cells of thickness 10 μm or even less. In smectic A (SmA), the molecules within the layers show fluid-like arrangement, with no long-range in-plane positional order; it is a uniaxial medium with the optic axis and $\mathbf{n}$ perpendicular to the layers. Other types of smectics show in-plane order; we do not consider them here.

2. Experimental observations of LC structures

Probing liquid crystals with light historically greatly contributed to our understanding of their structural properties, including defects. Below we consider basic principles of two techniques used to image defects in liquid crystals: the classic technique of polarizing microscopy [13, 1] and relatively new technique of fluorescence confocal polarizing microscopy.

2.1 Polarizing Microscopy of Liquid Crystals

Consider a UN slab sandwiched between two glass plates and placed between two crossed polarizers. The director $\mathbf{n}$ is in plane of the slab (Fig. 1) and depends on the in-plane coordinates (x,y). The light beam impinges normally on the cell, along the axis z. A polarizer placed between the source of light and the sample makes the impinging light linearly polarized. In the nematic, the linearly polarized wave of amplitude A, and intensity $I_0 = A^2$ splits into the ordinary and extraordinary waves with mutually perpendicular polarizations and amplitudes $A\sin\beta$ and $A\cos\beta$, respectively; $\beta\,(x,y)$ is the angle between the local $\mathbf{n}\,(x,y)$ and the polarization $\mathbf{P}$ of incident light. The vibration of the electric vectors at the point of entry are in phase. However, the two waves take different times, $n_o d/c$ and $n_e d/c$, respectively, to pass through the slab. Here n_o and n_e are the ordinary and extraordinary indices of refraction, d is the cell thickness and c is the speed of light in vacuum. At the exit point, the electric vibrations $A\sin\beta\cos\left(\omega t - \frac{2\pi}{\lambda_0}n_o d\right)$ and $A\cos\beta\cos\left(\omega t - \frac{2\pi}{\lambda_0}n_e d\right)$ gain a phase shift $\Delta\Phi = \frac{2\pi d}{\lambda_0}\,(n_o - n_e)$, where λ_0 is the wavelength in vacuum. The projections of these two vibrations onto the polarization direction of the analyzer behind the sample are of the same frequency and occur along the same directions. The analyzer thus transforms the pattern of (x,y)-dependent phase difference into the pattern of transmitted light intensity, that is easy to calculate from the consideration above:

$$I = I_0 \sin^2 2\beta \sin^2\left[\frac{\pi d}{\lambda_0}\,(n_e - n_o)\right] \qquad (1)$$

The last formula refers to the case when $\mathbf{n}$ is perpendicular to the axis z. If $\mathbf{n}$ makes an angle $\theta(z)$ with the axis z, then

$$I = I_0 \sin^2 2\beta \sin^2 \int_0^d \left[\frac{\pi}{\lambda_0} \left(\frac{n_o n_e}{\sqrt{n_e^2 \cos^2\theta + n_o^2 \sin^2\theta}} - n_o \right) \right] dz \quad (2)$$

Equations (1,2) represent only a rough approximation to the problem of light propagation in a birefringent medium. In general case of 3D distortions, one has to take into account that the extraordinary wave in the medium deviates from a straight line; one of the consequences is that a disclination line might create a "shadow," a region in which the extraordinary light does not enter [1]; such a disclination would appear to have a dark core much wider than the actual core. Nevertheless, Eqs. (1,2) are useful in understanding the LC textures. First, note that the phase shift and thus I depend on λ_0. As a result, when a thin sample is illuminated with a white light, it would show a colorful texture. The interference colors are especially pronounced when $(n_e - n_o)\, d \approx (1 \div 3)\, \lambda_0$. Second, the director tilt greatly changes the phase shift. When $\theta = 0$ (the so-called homeotropic orientation, $\mathbf{n} \| \hat{z}$), the sample looks dark, $I = 0$. Third, if $|\theta| > 0$ but $\beta = 0, \pm\pi/2, ...$, one might still observe dark textures, $I = 0$, even in nonmonochromatic light. In a sample with in-plane director distortions $\mathbf{n}(x, y)$, wherever $\mathbf{n}$ (or its horizontal projection) is parallel or perpendicular to the polarizer, the propagating mode is either pure extraordinary or pure ordinary and the corresponding region of the texture appears dark. Figure 2 is an example of such a texture with dark "brushes of extinction." Points at which the brushes converge are centers of topological defects (so-called boojums in this case). The texture with defects and dark brushes is called the Schlieren texture.

A polarizing microscopy image bears only a two-dimensional (2D) information, integrating the 3D pattern of optical birefringence over the path of light, see Eq.(2). The recently developed Fluorescence Confocal Polarizing Microscopy (FCPM) [14, 15] allows one to visualize the whole 3D director structure.

FCPM is a particluar mode of the confocal microscopy (CM). In CM, the sample region inspected at a time is a small (submicron) voxel (=3D pixel) [16]. Signals from nearby voxels are suppressed by a special (confocal) optical design with a pinhole in the image space. The point source of light, the inspected voxel and the pinhole are confocal. Light coming from the neighborhood of the inspected voxel is blocked from reaching the detector [16]. To obtain a 3D image of the whole sample, the tightly focused laser beam scans the specimen voxel by voxel. Using a computer, the data that describe an essen-

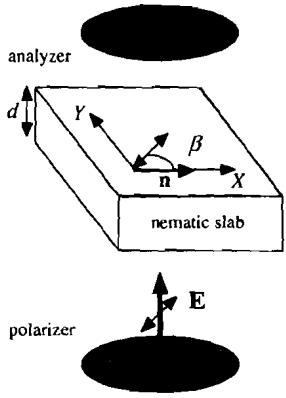

Figure 1. Light transmission through a nematic slab viewed between two crossed polarizers.

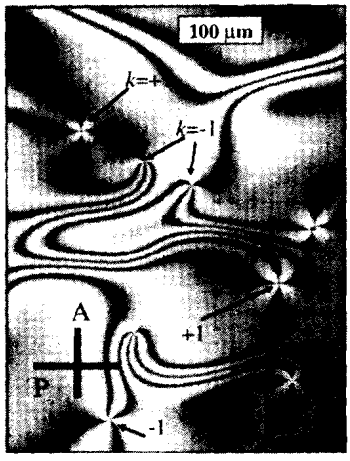

Figure 2. Schlieren texture of a uniaxial nematic LC under a polarizing microscope; nematic film (material: pentylcyanobiphenyl) of a thickness approximately 1 micron placed onto a glycerin substrate. Arrows indicate the core regions of the surface defects-boojums with topological charges k= -1 and k=+1.

tially 3D pattern, can be presented as a horizontal or vertical "cross-sections" of the sample.

FCPM adds two distinctive features to CM: (1) the liquid crystal under examination is doped with an anisometric fluorescent probe that is aligned by the host medium; (2) observation is performed in polarized (usually linearly) light [14, 15]. A simple view of how the FCPM visualizes a 3D director field in a nematic sample is as follows.

Imagine a UN composed of elongated molecules and doped with anisometric fluorescent dye molecules. The transition dipoles of both excitation and fluorescence align along $\mathbf{n}$. The linearly polarized incident light causes fluorescence of the dye. The efficiency of light absorption is determined by the angle between the polarization $\mathbf{P}$ of incident light and the direction of the absorption transition dipole of the dye molecule, i.e., $\mathbf{n}$. The excited dye fluoresces. The intensity of light detected through another polarizer (or the same one, in case of the reflective mode) depends on the angle between the polarizer and the emission transition dipole of the dye. In many cases, the resulting intensity is a steep function of the angle α between $\mathbf{n}$ and $\mathbf{P}$: [14, 15]

$$I \sim (\mathbf{n} \cdot \mathbf{P})^4 \sim \cos^4 \alpha. \tag{3}$$

Note that in the polarizing microscopy, two complementary director fields that differ everywhere by an angle $\beta = \pi/2$, are not resolved (a quaterplate or a quarz plate is needed in the optical pathway of the microscope). Such a problem does not exist in FCPM; however, one should be aware that the angle α defines a cone of directions; the degeneracy can be lifted by making observations with different settings of $\mathbf{P}$.

Apparently, the best resolution of the reflective mode FCPM, close to 0.5 μm, can be obtained in the vicinity of the entry plane. As the penetration inside the birefringent volume increases, the resolution worsens because of the spatial defocusing of the ordinary and extraordinary modes. This defocusing can be estimated roughly as [14, 15] $\Delta z_{anis} \sim g \Delta n z / n_{ave}$, where n_{ave} is the average refractive index, z is the depth of scanning (penetration), and g is a coefficient of the order of unity (dependent on the sample orientation, objective, and the director field). For a 20 μm depth of focusing and $\Delta n / n_{ave} \sim 0.05$, the defocusing is of the order of 1 μm; the lower the birefringence Δn of the liquid crystal, the better. Figure 3 shows the basic idea of FCPM technique, while Fig.4 demponstrates a vertical cross-section of a cholesteric liquid crystal sample, in which an edge dislocation is attracted to the top substrate [17].

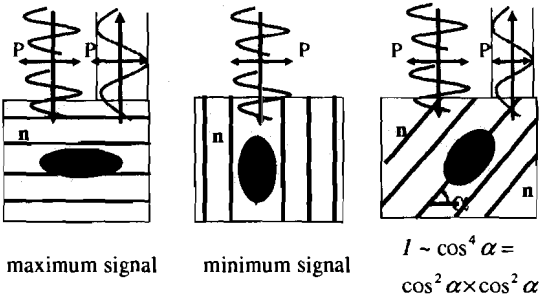

Figure 3. Principle of visualizing 3D director configuration in FCPM. The fluorescent dye molecules (ellipsoids) are aligned by the director. Polarized probing beam excites the dye molecules and cause fluorescence. The efficiency of excitation depends on the angle between the transition dipole of dye molecule (double-headed arrows) and polarization of probing beam.

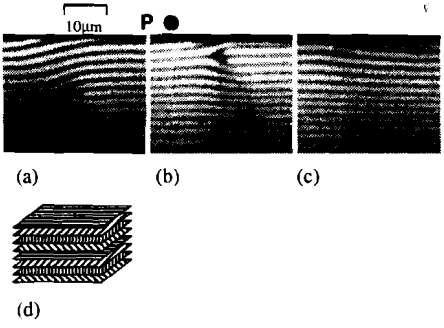

Figure 4. Fluorescence confocal polarizing microscope images of the edge dislocation in a cholesteric liquid crystal bulk (a) climbing towards the upper plate (b,c) with a weak surface anchoring. Part (d) shows structure of an unperturbed cholesteric liquid crystal with helicoidal twist of the director (straight lines).

3. Defects in nematics

3.1 Topological classification

The language of homotopy groups [18, 19] is the natural way to classify topological defects in media such as nematic LCs, to associate the character of ordering of a medium and the types of defects arising in it, to find the laws of

decay, merger and crossing of defects, to trace out their behavior during phase transitions, etc. The key concept is that of a topological invariant, or topological charge, inherent in every defect. Stability of the defect is guaranteed by the conservation of its charge. Homotopy classification of defects implies three steps.

First, one defines the order parameter (OP) of the system; its amplitude and phase. For example, director can be considered as the phase of the nematic order parameter; it is also called a degeneracy parameter as reorientations of $\mathbf{n}(\mathbf{r})$ as the whole does not change the thermodynamical potentials of the system.

Second, one determines the OP (or degeneracy) space R, i.e., the manifold of all possible values of the OP that do not alter the thermodynamical potentials of the system. In the uniaxial nematic R is a sphere S^2/Z_2 with pairs of diametrically opposite points being identical. Every point of S^2/Z_2 represents a particular orientation of $\mathbf{n}$. Since $\mathbf{n} \equiv -\mathbf{n}$, any two diametrically opposite points at S^2/Z_2 describe the same state.

The function $\mathbf{n}(\mathbf{r})$ maps the points of the nematic volume into S^2/Z_2. The mappings of interest are those of i-dimensional 'spheres' enclosing defects. A line defect is enclosed by a loop, $i = 1$; a point defect is enclosed by a sphere, $i = 2$, etc.

Third, one defines the homotopy groups $\pi_i(R)$. The elements of these groups are mappings of i-dimensional spheres enclosing the defect in real space into the OP space. To classify the defects of dimensionality t' in a t-dimensional medium, one has to know the homotopy group with $i = t - t' - 1$.

On the one hand, each element of $\pi_i(R)$ corresponds to a class of topologically stable defects; all these defects are equivalent to one another under continuous deformations. On the other hand, the elements of homotopy groups are topological charges of the defects. The defect-free state corresponds to a unit element of the homotopy group and to zero topological charge. The results of the homotopy classification for UN and BN are as follows.

UN. There are no stable walls, as $\pi_0(S^2/Z_2) = 0$. There is one class of topologically stable line defects (disclinations), as $\pi_1(S^2/Z_2) = Z_2 = (0, 1/2)$. The addition rules for defect combinations are $1/2 + 1/2 = 0, 1/2 + 0 = 1/2$; the only stable disclinations are those that correspond to the element $1/2$.

It is customary to characterize the disclinations with a special integer or semi-integer number k called the strength. It shows how many times the director rotates by 2π when one circumnavigates the defect core once. The sign of k indicates the director of rotation; it has no topological relevance, as the states with opposite signs are topologically equivalent. The difference between stable lines of, say, $k = 1/2$ and $k = -1/2$, is energetical rather than topological, as they can be continuously transformed one into another. Besides,

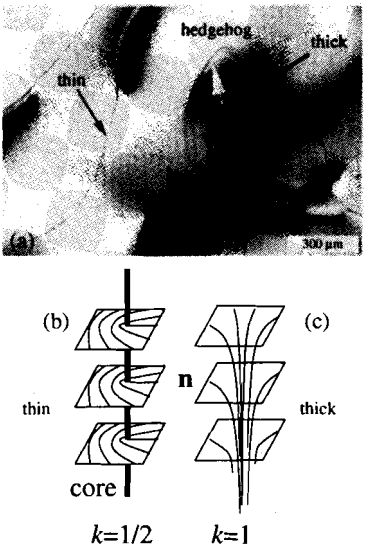

Figure 5. Singular (thin, half-integer k) and nonsingular (thick, integer k) disclination lines and point defect-hedgehog along the non-singular disclination as seen in the bulk of a nematic slab under the polarizing microscope (a). Part (b) and (c) show the director congifurations around thin and thick disclinations, respectively.

all lines with $|k| = 1/2 + n$, where n is an integer, are topologically equivalent to each other, as are the lines with $|k| = n$. Energetically, as we shall see later, smaller values of n are preferrable. The stable $|k| = 1/2$ lines are often referred to as "thin" lines, while $|k| = 1$ as "thick" lines. The terminology is explained by the appearance of the defect cores under the microscope, Fig.5: the cores of $|k| = 1/2$ lines are singular while $|k| = 1$ defects are non-singular.

There are stable point defects, the so-called hedgehogs, as $\pi_2\left(S^2/Z_2\right) = Z = (0, \pm 1, \pm 2, ...)$. As $\mathbf{n} = -\mathbf{n}$, each point defect can be equally labeled by the topological invariant N and $-N$ [19]:

$$N = \frac{1}{4\pi} \int \int \mathbf{n} \left[\frac{\partial \mathbf{n}}{\partial u} \times \frac{\partial \mathbf{n}}{\partial v} \right] dudv, \tag{4}$$

where u and v are the coordinates specified on the sphere S^2 surrounding the point defect.

Besides hedgehogs, there is another type of point defects in the nematic phase, so-called boojums, Fig.6,7. Boojums, in contrast to hedgehogs, can exist only at the boundary of the medium [20], Fig.2,6,7. The core of the boodjum is located at the boundary or at some distance from it (a virtual core), if the surface anchoring strength is finite (which is always the case in practice), Fig.6. In addition to the integer N, boojums in a uniaxial nematic

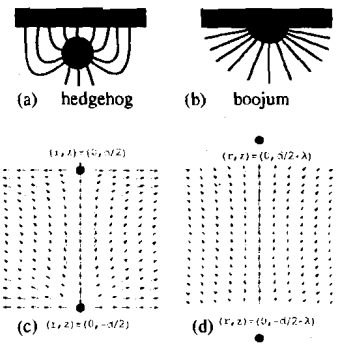

Figure 6. Point defect-hedgehog in the UN bulk (a) and point defect-boojum at the UN surface (b); pairs of boojums at the opposite sides of the flat nematic sample (c,d); their cores are located at the bounding plates in the case of infinitely strong tangential anchoring (c), or at some distance $\lambda \tilde{} K/W$ from the plate for a finite anchoring coefficent W; K is the typical elastic curvature (Frank) constant of the UN.

can be characterized by a 'two-dimensional' topological charge k of the unit vector field $\tau = \mathbf{n} - \nu\,(\mathbf{n} \cdot \nu)$ projected by the director onto the boundary: $k = \frac{1}{2\pi} \int\int \left(\tau_x \frac{\partial \tau_y}{\partial u} - \tau_y \frac{\partial \tau_x}{\partial u}\right) ds = 0, \pm 1, \pm 2, ...$, where s is the natural parameter defined along the loop at the bounding interface enclosing the defect core; similarly to the case of disclinations, k shows how many times τ rotates by 2π when one circumnavigates the defect once [21]. Boojums are characterized by elements of the relative homotopic group $\pi_2\left(S^2/Z_2, \mathcal{R}_s\right)$, where $\mathcal{R}_s$ is the degeneracy space of the system at the surface that depends on the type of director orientation there: $\mathcal{R}_s = 0$ when the equilibrium angle θ_0 between $\mathbf{n}$ and the normal ν to it is 0; $\mathcal{R}_s = S^1$ when $0 < \theta_0 < \pi/2$, and $\mathcal{R}_s = S^1/Z_2$ when $\theta_0 = \pi/2$ [21]. The phenomenon that sets an equilibrium value of θ_0 at the surface of a liquid crystal is called anchoring; it stems from the broken symmetry of molecular interactions near an interface; we will return to this phenomenon later on.

In a nematic film confined between two glass plates, with the director being in the plane of the sample, $\theta_0 = \pi/2$, one can observe two types of apparently point defects: those with $k = \pm 1/2$ that actually are the ends of line disclinations connecting the opposite glass plates, and the true point defects-boojums with $k = \pm 1$, Fig.7. In practice, to distinguish the two, it suffices to shift

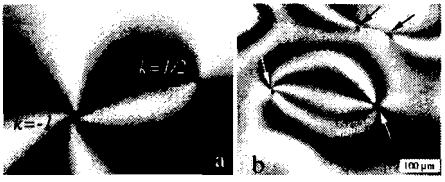

Figure 7. A polarizing-microscope texture of a nematic slab (a) reveals two types of apparently point-like defects at the bpounding plates: the centers with two dark brushes and thus $k = \pm 1/2$ and the centers with four dark brushes and thus $k = \pm 1$. Shifting of the two glass plates with respect to each other (b) shows that the two types of surface point-like defects are in fact very different: $k = \pm 1/2$ defects represent the ends (black arrows) of the line defects-disclination connecting the two glass plates and $k = \pm 1$ centers represent the true surface point defects-boojums (white arrows); when separated, they leave a non-singular fuzzy trace in the nematic bulk.

the plates of the cell with respect to each other, Fig.7b: the separated boojums leaves a non-singular trace between them, while the ends of disclination will appear connected by the defect line.

BN. In the biaxial nematics, there are no hedgehogs, and there are five topological classes of disclinations [22], $\pi_1 (SO(3)/D_2) = Q$, where Q is the group of quaternion units. Defects $k = \pm 1$ are topologically stable [22]: the escape does not remove the singular core, as upon reorientation of one of the directors $\mathbf{n}$, $\mathbf{l}$, and $\mathbf{m}$ into an escaped configuration, another two restore the singularity. However, if two out of the three directors are associated with small Frank constants (which should occur in the vicinity of the N-BN traqsition), the escape of the "hardest" of the tree directors is possible [23]. Some pairs of disclinations cannot cross each other without creation of a third disclination that joins the original pair [22, 1].

3.2 Disclination textures

When a thick UN sample is viewed under the microscope, the disclinations are seen as thin and thick threads, Fig.5. Thin threads strongly scatter light and show up as sharp lines. These are true topologically stable disclinations, along which the nematic symmetry of rotation is broken. Thick threads are line defects only in appearance; they are not singular disclinations. The director is smoothly curved and well defined everywhere; it can be, at least in

principle, transformed into a uniform state; the obstacles might be imposed by the conditions at the walls of the sample or by other defects.

In thin UN samples (1-50 μm), the threads are often perpendicular to the bounding plates, as in Fig.7a. Under a polarizing microscope, the threads show up as centers with emanating dark brushes, giving rise to the Schlieren texture, Fig.2 and Fig.7. The dark brushes display the areas where $\mathbf{n}$ is either in the plane of polarization of light or in the perpendicular plane. There are usually two types of centers: with two and four dark brushes, Fig.7. They correspond to the thin and thick threads, respectively.

The centers with two dark bands have a sharp (singular) core, insofar as can be seen, of sub-micrometer dimensions and correspond to the ends of singular stable disclinations, Fig.7b. The director rotates by π when one goes around such a center. Presence of centers with two brushes signals that $\mathbf{n}$ is parallel to the bounding plates: the in-plane rotation brings the director $\mathbf{n}$ into its equivalent state $-\mathbf{n}$. A small change in boundary conditions leads to symmetry breaking: if the angle between $\mathbf{n}$ and the substrate is different from zero, then the projection of the director $\mathbf{n}_s$ onto the bounding plates does not satisfy the condition $\mathbf{n}_s = -\mathbf{n}_s$. The centers with four brushes in Fig.2, 7 correspond to isolated point defects, boojums. One can observe the difference between the two-brushes and four brushes centers by gently shifting one of the bounding plates, Fig.7b. On rare occasions, centers with number of brushes higher than four are encountered. These observations signal some peculiarity of the nematic material [24] or of the boundary conditions [25].

Equations (1,2) allow one to relate the number k of director rotation by 2π around the defect core, to the number B of brushes emanating from the core in the Schlieren texture, $|k| = B/4$. Note, however, that the last equality is valid only when the rate of director rotation around the core does not change sign. In some textures, especially when the centers show more than four brushes, this restriction is not satisfied and there is no simple relationship between $|k|$ and B, see [25] for details.

3.3 Elasticity

In the so-called Frank-Oseen model of nematic and cholesteric LCs, the free energy (volume) density of elastic distortions f_{el} is written as an invariant quadratic form of the first spatial derivatives of $\mathbf{n}$ [1]:

$$f_{el} = f_{FO} = \frac{K_{11}}{2}(\mathrm{div}\mathbf{n})^2 + \frac{K_{22}}{2}(\mathbf{n}\cdot\mathrm{curl}\mathbf{n})^2 + K_c(\mathbf{n}\cdot\mathrm{curl}\mathbf{n}) + \frac{K_{33}}{2}[\mathbf{n}\times\mathrm{curl}\mathbf{n}]^2 - K_{24}\,\mathrm{div}(\mathbf{n}\cdot\mathrm{div}\mathbf{n} + \mathbf{n}\times\mathrm{curl}\mathbf{n}), \quad (5)$$

where K_{11}, K_{22}, and K_{33} are the "bulk" Frank elastic constants for splay, twist, and bend deformations, respectively, K_c is the chiral coefficient that

determines the pitch of cholesteric LC: $p = 2\pi K_{22}/K_c$; $p \to \infty$ in the nematic LC. The divergence (often called saddle-splay or "surface-like") elastic K_{24} term can be reduced to the surface integral but has to be taken into account when the topology of director distribution changes; note that here we neglect another divergence term K_{13} div $(\mathbf{n}\cdot\text{div}\mathbf{n})$ by assuming $K_{13} = 0$.

The divergence nature of the K_{24} term allows one to transform the volume integral

$$\int K_{24}\,\text{div}\,(\mathbf{n}\cdot\text{div}\mathbf{n} + \mathbf{n}\times\text{curl}\mathbf{n})dV = K_{24}\int\int \nu\cdot(\mathbf{n}\cdot\text{div}\mathbf{n} + \mathbf{n}\times\text{curl}\mathbf{n})dA, \tag{6}$$

at least away from the interfaces and defect cores, when the modulus K_{24} is constant. However, whatever the way of integration of this term, the resulting energy scales similarly to the elastic energy of the regular "bulk" terms, usually linearly with the system size. The difference between K_{24} and other terms is more subtle: the divergence term does not enter the Euler-Lagrange equations for equilibrium in the bulk, but it influences the equilibrium director through the boundary conditions (which might be imposed also at the core of defects). It should be taken into consideration when the topology of the defect states changes, as, for example, in the hedgehog-loop or radial-hyperbolic hedgehog transformations, see below.

Frank in 1958 [26] considered the equilibrium defects configurations corresponding to the free energy density above. He assumed that (1) the director field is twistless and that it is everywhere parpendicular to the axis of line defet (the so-called 'planar' disclinations), $\mathbf{n} = [\cos\psi,\ \sin\psi, 0]$, where φ is the function of the Cartesian coordinates, $\psi(x, y)$, or polar coordinates, $\psi(r, \varphi)$; (2) the bulk elastic constants are equal, $K_{11} = K_{33} = K$. Note that in planar case, the K_{24}-term in the line's energy is zero. The Euler-Lagrange equation in the Frank model is the same as the 2D Laplace equation of electrostatics, $\Delta\psi = 0$, which writes in polar coordinates as

$$\frac{1}{r}\frac{\partial}{\partial r}\left(r\frac{\partial\psi}{\partial r}\right) + \frac{1}{r^2}\frac{\partial^2\psi}{\partial\varphi^2} = 0. \tag{7}$$

One of the classes of singular solutions is $\psi = A\varphi + B(r, \varphi)$, where A is a constant, and $B(r, \varphi)$ is the harmonic regular function at the origin. From the condition $\int_C d\psi = 2\pi k$, one finds $A = k$, where $k = 0, 1/2, \pm 1, ...$is the disclination "strength." The elastic energy per unit length

$$F_{1l} = \frac{1}{2}K\int(\nabla\psi)^2\,dxdy^{\sim}\int r^{-1}dr \tag{8}$$

is logarithmically divergent:

$$F_{1l} = \pi K k^2 \ln\frac{R}{r_c} + F_c, \tag{9}$$

where R is the characteristic size of the system, r_c and F_c are respectively the radius and the energy of the disclination core, a region in which the distortions are too strong to be described by a phenomenological theory. The energy of two parallel planar disclinations separated by a distance L, $r_c << L << R$, is [1]

$$F_{12} = \pi K (k_1 + k_2) \ln \frac{R}{r_c} - 2\pi K k_1 k_2 \ln \frac{L}{2r_c}. \qquad (10)$$

The Frank theory does not distinguish lines of integer and semi-integer k, except for the fact that the lines with $k = \pm 1$ tend to split into pairs of lines $k = \pm 1/2$, which often reduces the energy, as $F_{1l} - F_c \tilde{} k^2$. Anisimov and Dzyaloshinskii in 1972 [27] showed that, in additional to planar lines, non-planar, or 'bulk' stable disclinations with $k = \pm 1/2$ can exist, in which the director does not lie in a single plane.

The lines of integer k, as predicted by the homotopy theory, are fundamentally unstable. Imagine a circular cylinder with normal orientation of at the boundaries, Fig.8a. The planar disclination would have a radial-like director field normal to the axis of the cylinder, $k = 1$. However, the director can be re-oriented along the axis. This 'escape into the third dimension' is energetically favorable, since the energy of the escaped configuration is only $F_{1l} = 3\pi K$. [28]; [29]. When opposite directions of the 'escape' meet, a point defect-hedgehog is formed, Fig.8c. The tendency to escape is preserved even when the disclination with integer k is formed between two flat plates that set tangential director orientation, as in Fig.8, at least for the realistic values of the surface anchoring coefficient ($W \tilde{} 10^{-4} J/m^2$, see below) and thickness of the slab larger than 1 μm [23]. The escape in a flat cell leaves two boojums, as shown in Fig.6c,d. Note that with typical $W \tilde{} 10^{-4} J/m^2$ and elastic constant $K \tilde{} 10^{-11} N$, the characteristic anchoring length $\lambda = W/K$ is relatively small, of the order of $0.1 \mu m$, and one can assume that the core of the boojum is located closely to the bounding plate, see Fig.6d.

Unlike point defects such as vacancies in solids, the topological point defects in uniaxial nematics cause disturbances over the whole volume. The curvature energy of the point defect is proportional to the size of the system. For example, for a radial hedgehog $\mathbf{n} = (x, y, z) / \sqrt{x^2 + y^2 + z^2}$,

$$F_{rh} = 8\pi R (K_{11} - K_{24}) + F_{cr}, \qquad (11)$$

and for a hyperbolic one, $\mathbf{n} = (-x, -y, z) / \sqrt{x^2 + y^2 + z^2}$,

$$F_{hh} = 8\pi R \left(\frac{K_{11}}{5} + \frac{2K_{33}}{15} + \frac{K_{24}}{3} \right) + F_{ch}. \qquad (12)$$

Stability of the particular defect configuration might depend on the values of the elastic constants. For example, the point defect might spread into a topo-

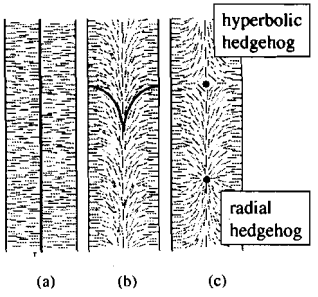

Figure 8. Disclination $k = 1$ in a circular cylinder with normal boundary condition (a) is unstable against the escape into third dimension (b); the effects might lead to formation of point defects - hedgegogs (c).

logically equivalent disclination of $k = \pm 1/2$, [30], Fig.9. Note that, unlike in the case of planar disclinations, the divergence K_{24}-term does contribute to the energies of the hedgehogs (see the last two equations) and loops. For example, the K_{24}-term contributes $(-8\pi K_{24} R)$ to the energy of the radial hedgehog. If such a point defect transforms into a topologically equivalent circular loop with $k = 1/2$, then its energy is [31]

$$F_{loop} = 8\pi R\,(K - K_{24}) + 2\pi^2 K_{24} a + \frac{\pi^2}{2} aK \left[\ln \frac{a}{2r_c} - 5 + \frac{4}{\pi} f_{cl}\right], \quad (13)$$

where a is the radius of the ring, $f_{cl} = F_{cl}\xi^2/K$, F_{cl} is the loop core energy, ξ is the nematic coherence length. Here, to elucidate the role of K_{24}, we assume that the two relevant bulk elastic constants are equal, $K_{11} = K_{33} = K$. Minimization yields the equilibrium value of the loop radius that strongly depends on K_{24} [31]:

$$a^* = 2r_c\,(4 - 4K_{24}/K - 4f_{cl}/\pi) \approx 30\xi \exp\left[-\frac{4K_{24}}{K}\right]. \quad (14)$$

In UN, the disclinations can always pass through each other. They can exchange ends (reconnection) or not, depending on the original geometry, as documented experimentally [32], see Fig.10. In BN, some pairs of disclinations produce a third line when passing through each other [22].

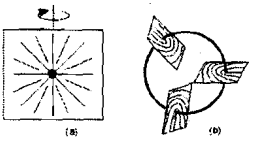

Figure 9. A point defect - hedgehog transforms into a disclination loop.

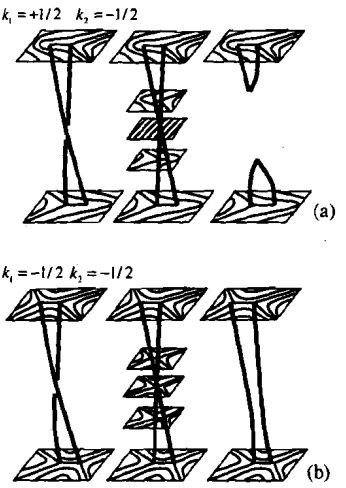

Figure 10. (a) Two disclinations of the opposite sign with ends fixed at two surfaces recombine and disconnect in the horizontal plane, shortening the total length of the defects pair. (b) Two disclinations of the same sign with ends fixed at two surfaces recombine and disconnect in the vertical plane, leaving the total length practically the same.

3.4 Surface anchoring phenomena; Equilibrium point defects in nematic droplets

When left intact, textures with defects in flat samples relax into a more or less uniform state. Disclinations with positive and negative k find each other, reconnect and annihilate, thus reducing the total length of disclinations web. There are, however, situations when the equilibrium state requires topological defects. The defects are brought about by the effects of surface anchoring.

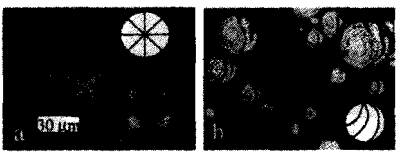

Figure 11. Because of the difference in surface anchoring conditions, nematic (UN) droplets freely suspended in the glycerin doped with lecithin (a) and in pure glycerin (b) exibit different director structures. The structures contain equilibrium topological defects, either a pint defect-hedgehog in the center of the droplet (a) or a pair of surface point defects-boojums at the poles (b). The easy axis is normal to the interface in (a) and tangential to the interface in (b). Note that the droplets with tangential anchoring (b) have a twisted director structure and are thus optically active; the effect is caused by the smallness of the twist elastic constant as compared to the bend and splay elastic constants.

Broken symmetry of molecular interactions at the boundary lifts the degeneracy of director orientation in space and sets some weel-defined direction(s) of $\mathbf{n}$, called the "easy axis (axes)." The easy axis might be perpendicular to the surface ("homeotropic alignment"), tilted, tangential, uniaxial tangential (called also "planar"), etc. An easy axis can be created by the geometry of the system even when the bounding plates are "isotropic". For example, imagine a tangentially anchored UN confined between two plates. Any direction of $\mathbf{n}$, as long as it is parallel to the plates, would correspond to the equilibrium state. However, if the plates are tilted with respect to each other, then the equilibrium orientation would be along the thickness gradient; all other directions would imply director distortions [33]. The phenomenon, called "geometrical anchoring," might lead to the appearance of twisted director configurations [33].

Nematic droplets suspended in an isotropic matrix such as glycerin, water, polymer, etc. [21, 34], or nucleating during the first-order isotropic-nematic phase transition, and inverted systems, such as water droplets in a nematic matrix [35] are the most evident examples in which the surface anchoring might result in equilibrium defect structures, Fig.11.

The equilibrium structure in a bounded volume is found by minimizing the total free energy functional F, which is a sum of the elastic (we consider field-free situations) and the surface energies. The later is comprised of the isotropic (surface tension) and anisotropic (surface anchoring) terms. Usually, the surface tension coefficient $\sigma^{\sim} \left(10^{-2} - 10^{-3}\right) J/m^2$ is much large than its

anchoring counterpart $W \sim (10^{-4} - 10^{-6})\ J/m^2$, and a liquid crystal droplet suspended in a suitable matrix (say, glycerin or the melt of the liquid crystal itself in the biphasic region; the liquid crystal and the matrix have a similar densities) adopts a spherical shape. The anchoring coefficient W is the measure of work one needs to spend to deviate the director from the easy axis by a certain angle, say, $\pi/2$ in the so-called Rapini-Papoular model; the area of the interface is fixed. Experimentally, it can be determined by measuring director reorientation under the action of an external field [36].

The minimization problem for a body with a fixed shape involves not only the elastic energy $\int_V f_{el} \mathrm{d}V$ functional, but also the surface anchoring energy $\int_S f_S \,\mathrm{d}S$:

$$F = \int_V f_{el} \mathrm{d}V + \int_S f_S \,\mathrm{d}S; \tag{15}$$

If the liquid crystal is adjacent to an isotropic medium and molecular interactions at the interface set strictly normal or tangential boundary conditions, one often uses the so-called Rapini-Papoular anchoring potential [37]:

$$f_s = \frac{1}{2} W (\mathbf{n} \cdot \nu)^2, \tag{16}$$

where ν is the unit normal to the liquid crystal-ambient medium interface; the anchoring coefficient $W > 0$ for tangential boundary conditions and $W < 0$ for normal boundary conditions. More generally,

$$f_s = -\frac{1}{2} W_{ij}\, n_i\, n_j, \tag{17}$$

where W_{ij} is the symmetrical anchoring tensor, that describes the easy axis as well as polar and azimuthal anchoring coefficients [38].

Consider a spherical nematic droplet of a radius R. The isotropic surface energy scales as σR^2, the surface anchoring energy scales as $|W| R^2$ and the elastic energy as KR; here $K \sim 10^{-11} N$ is some averaged Frank constant. Practically any macroscopic droplet is spherical, as $K/\sigma \sim (1 - 10)\, nm$. Small droplets with $R << K/|W|$ avoid spatial variations of $\mathbf{n}$ at the expense of violated boundary conditions. In contrast, large droplets, $R >> K/|W|$, satisfy boundary conditions by aligning $\mathbf{n}$ along the preferred direction(s) at the surface. In a spherical droplet, the result is the distorted director in the bulk, for example, a radial point defect-hedgehog when the surface orientation is normal, Fig.11a. Note that the characteristic radius $R_c = K/|W|$ is macroscopic (0.1-10 microns), as $|W| \sim (10^{-4} - 10^{-6})\ J/m^2$.

Point defects (both hedgehogs and boojums) in large systems such as nematic droplets with $R >> K/|W|$, must satisfy restrictions

$$\sum_i k_i = E \text{ and } \sum_j N_j = \frac{1}{2}E\,, \tag{18}$$

The first relationship is the Poincare theorem: the sum of the indices of the vector field defined at a surface is equal to the Euler characteristic E of this surface. For a sphere E=2 and for a torus E=0. The second equality in Eq.(18) is a consequence of the Gauss theorem and the fact that defects such as hedgehogs can exist not only in the bulk but at the surface as well [21].

The simplest example of the equilibrium defect structures can be easily found in sufficiently large spherical UN droplets freely suspended in a suitable isotropic matrix: a spherical droplet with perpendicular anchoring shows a single hedgehog at the center, while a droplet with tangential director anchoring shows two boojums at the poles, Fig.11. By changing the direction of the easy axis from normal to tangential (or vice versa), one can observe "topological dymamics" of defects, in which a hedgehog is replaced by the pair of boojums; the process involves disclination loops, see [21]. Another interesting illustration of Eq.(18) are "Dirac monopole" structures that represent a combination of a hedgehog and a disclination line emanating from the center of the point defect, and can be easily observed in liquid crystals of the smectic C [39] or cholesteric type.

The conservation laws given by Eqs. (18) may influence the late stages of the first-order isotropic-to-nematic phase transition that occurs through nucleation of nematic droplets. The critical radius of nucleation is (see, for example, [1]) $r_c = 2\sigma/f$, where $\sigma \tilde{} 10^{-5} J/m^2$ [7] is the surface tension coefficient for the isotropic-nematic interface, and f is the bulk energy density difference between the isotropic and nematic phases. Estimating $f \tilde{} \Delta T \Delta H / T_{NI}$, where $\Delta T = T_{NI} - T$ is the depth of temperature quench and $\Delta H \tilde{} 10^5 J/m^3$ is the latent heat of transition [40], one finds $r_c \tilde{} 0.01\ \mu m$ for deep quenches (tens of degerees), $r_c \tilde{} 0.1\ \mu m$ when the quench is a degree or so below the transition temperature T_{NI} and $r \to \infty$ when $T \to T_{NI}$. The droplets grow by adding molecules from the isotropic matrix and by coalescence. At early stages of deep quench, small droplets are practically uniform; they might form defects upon coalescence according to the Kibble mechanism. However, as soon as the droplets grow above $R_c = K/|W|$, a more powerful deterministic source comes into play, namely, surface anchoring and the topological constraints considered above. For the popular nematic material pentylcyanobiphenyl (5CB), the surface anchoring coefficient at the nematic-isotropic interface has been measured to be $|W| \approx 10^{-6}\ J/m^2$ [7] while $K \approx 2 \times 10^{-12}\ J/m^2$ [8]. Therefore one might expect that the anchoring-induced production of defects becomes effective for $R > R_c \approx 2\mu m$. This is indeed what happens, Fig.12. Figure 12 shows nematic droplets growing from the isotropic melt (E7 mixture containing cyanobiphenyls, similar to 5CB): supramicron droplets clearly con-

tain stable topological defects. Because of the surface anchoring that favors tilted conical director orientation, there are both point defects and disclination loops; the corresponding director fields are described in details in Ref. [21]. The anchoring mechanism is extremely effective, producing one disclination loop per each nematic droplet of the appropriate size in the case of Fig.12b. Interestingly, Bowick et al. [9], expanding on the earlier studies [10], have discovered that the number of "strings" (disclinations) produced in the 5CB isotropic-nematic transition was about 0.6 per "bubble" (droplet). Although this number has been found to be in reasonable agreement with the Kibble mechanism [9], it might also signal a significant contribution of the anchoring mechanism. Really, as Fig.2b and 2c in Ref.[9] reveal, most of the droplets were at least 40 μm in diameter before the continuous nematic slab was formed. Therefore, the 5CB droplets should have satisfied the conditions for the anchoring-driven defect production ($R > R_c \approx 2\mu m$) and for the formation of boojums and loops (as the surface alignment is titled for 5CB [7]). The problem deserves further study, as the defect structure of droplets and possible presence of boojums and loops was not addressed in Ref. [9] (instead, the appearance of monopoles-hedgehogs has been suggested).

To summarize, the balance of Kibble and anchoring-driven defect production shown in Fig.12 during the isotropic-nematic phase transition is still an open problem. Clearly, it should strongly depend on the speed and depth of quenching; fast and deep quench that produces numerous sub-micron nuclei separated by submicron distances might mitigate the anchoring mechanism. On the other hand, slow quench might tell a story of anchoring-induced defect dynamics in growing droplets which is of interest on its own. These experiments are in progress.

4. Defects in SmA and other Lamellar Systems

4.1 Elasticity

The order parameter of SmA phase includes a nematic contribution (coming from the normal to the layers) and a 1D solid contribution. The nematic "bulk" part yields the same free energy as for UN (1,2), with no twist term, as in the system of layers, $\mathbf{n}\cdot\mathrm{curl}\mathbf{n} = 0$; the solid part yields a compressibility, or B-term, viz.

$$f_A = \frac{K_{11}}{2}\,(\mathrm{div}\mathbf{n})^2 + \frac{K_{33}}{2}\,[\mathbf{n}\times\mathrm{curl}\mathbf{n}]^2 - K_{24}\,\mathrm{div}\,(\mathbf{n}\cdot\mathrm{div}\mathbf{n} + \mathbf{n}\times\mathrm{curl}\mathbf{n}) + \frac{B}{2}\,\gamma^2, \tag{19}$$

where d_0 is the equilibrium repeat distance, d is the actual layer thickness measured along, $\gamma = (d - d_0)/d_0$ is the relative dilation, and B is the Young modulus for the 1D solid.

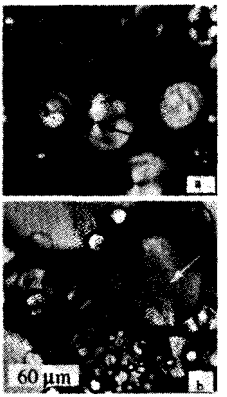

Figure 12. First-order isotropic-to-nematic phase transition in a nematic mixture E7 in a glass container of thickness 200 micron; biphasic region. Nematic nuclei-droplets show various defects such as boojums (black arrows) and disclination loops (white arrows) stabilized by surface anchoring at the nematic-isotropic interface. Parts (a,b) show the same sample; part (b) corresponds to the later stage of the phase transition as compared to part (a).

The ratio of K_{33} to B contributions is $\frac{(K_{33})}{(B)} \sim \frac{K_{33}}{B}\frac{1}{r^2} \sim \frac{\lambda_{33}^2}{r^2}$, where $\lambda_{33} = \sqrt{K_{33}/B}$ is some length of the order of d_0 and r is some characteristic radius of deformation. For macroscopic r, K_{33} contribution, which is a deformation associated with the layers compression, is negligible compared with the B-contribution, which is of the same nature. It is usually dropped, but we will see one example, in which K_{33} does appear to play a role, in the problem of cholesteric anchoring.

In many situations of practical interest, the departures of layers from an ideal equilibrium flat configuration are small and the expression for the elastic free energy density can be simplified by introducing a single scalar variable u, that describes the layer displacement field:

$$f_A = \frac{1}{2}K_1\left(\frac{\partial^2 u}{\partial x^2}\right)^2 + \frac{1}{2}B\left[\frac{\partial u}{\partial z} - \frac{1}{2}\left(\frac{\partial u}{\partial x}\right)^2\right]^2. \tag{20}$$

The ratio of the two elastic moduli defines an important length scale $\lambda = \sqrt{K_1/B}$, called the "penetration length" . The correction term $\left[-\frac{1}{2}\left(\frac{\partial u}{\partial x}\right)^2\right]$ makes the compression term invariant with respect to uniform rotations. A uniform rotation of layers, say, by an angle $\theta = \frac{\partial u}{\partial x}$, should not change the

energy. However, it changes the effective layer spacing measured along the fixed axis, $d_0 \rightarrow d_0/\cos\theta$. The effective strain is $d_0\,(1-1/\cos\theta)\,/d_0 \approx -\theta^2/2$, hece the correction term. Note that this term makes the theory non-linear.

The free energy density suitable to describe large bendings of layers and small dilations/compressions, is usually written in the form (see, e.g., [1])

$$f_A = \frac{1}{2}K_1\left(\frac{1}{R_1}+\frac{1}{R_2}\right)^2 + \overline{K}\frac{1}{R_1R_2} + \frac{1}{2}B\gamma^2, \qquad (21)$$

where $\overline{K}$ is the saddle-splay elastic constant , R_1 and R_2 are the principal radii of curvature. Note that for the director field n(r) defined as a unit normal to the layers,

$$\mathrm{div}\mathbf{n} = \pm\left(\frac{1}{R_1}+\frac{1}{R_2}\right); \qquad \mathrm{div}\,(\mathbf{n}\cdot\mathrm{div}\mathbf{n} + \mathbf{n}\times\mathrm{curl}\mathbf{n}) = \frac{2}{R_1R_2}. \quad (22)$$

Dimensional analysis suggests that for deformations at scales L much larger than the interlamellar spacing d_0, the curvature contribution $\tilde{}KL$ is much smaller than the bulk contribution $\tilde{}BL^3\tilde{}KL\left(\frac{L}{\lambda}\right)^2$, as $L >> d_0$. Therefore, at $L >> d_0$, one can treat the lamellar medium as a system of equidistant (and thus parallel) layers with predominantly curvature distortions.

Imagine now a confined volume of a lamellar phase. The layers are curved to satisfy the boundary conditions. As the layers tend to be parallel to each other, the centers of curvature form two focal 2D surfaces. The energy of the focal surfaces is large, $\tilde{}B\lambda L^2$. An efficient way to reduce this energy is to reduce the dimensionality of the focal surfaces, by shrinking them into lines or points. Clearly, the focal lines and the corresponding system of layers adopt only a selected set of shapes. One of the most often met situations is when the focal lines are a pair of cofocal ellipse and hyperbola; the limiting case is a circle with a straight line passing through its center [1]. The lamellae fold around the defect pair preserving their equidistance everywhere, except at the cores of the defects. They have the shape of Dupin cyclides, i.e. surfaces whose lines of curvature are circles. The structure is called a focal conic domain (FCD), Fig.13. In Fig.13, the line $M'M''$ represent one of the director lines; it connects the ellipse and the hyperbola; it is normal to all the layers it crosses. The layers of type "1" in Fig.13a,b, have cusps at the ellipse, the layers of type "3" have cusps on the hyperbola, while the layers of type "2" are non-singular.

A good model of the lamellar system is a cholesteric (Ch) phase, Fig.4d. Ch is formed by chiral nematogen molecules; molecular interactions lack inversion symmetry. The director is twisted into a uniaxial helix (although more

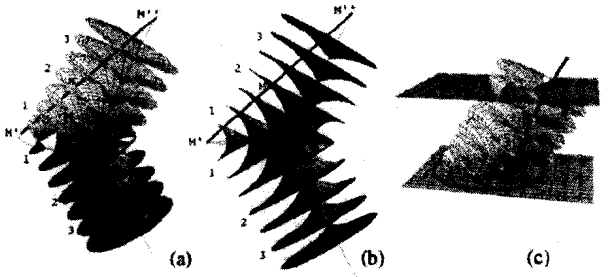

Figure 13. Focal conic domains based on a confocal ellipse-hyperbola pair. Surfaces correspond to equidistant layers. Parts (a,b) show the same FCD in the bulk viewed from different directions. Part (c) illustrates a FCD in a bounded sample with the elliptic base being on one of the plates. Note that within the base, the layers are perpendicular to the bottom plate; at the top plate, the layers are tilted.

complex geometries, such as blue phases with "double twist" are also possible). Spatial scale of background deformations, e.g., the pitch p of the helix, is normally much larger than the molecular size, as the interactions that break the inversion symmetry are weak. This feature makes Ch a very attractive lamellar medium to study defects: with p in the range of few microns, one can study defects in details using a standard microscopy or FCPM.

Elastic properties (and thus defects) at short-range and long-range (as compared to p) scales are different. The homotopy classification of defects is similar to that for biaxial nematics and predicts phenomena such as topological entanglement of disclinations and formation of non-singular soliton configurations [1]. However, periodic nature of director helix leads to a dual character of defects, as at large scales, one finds stable defects such as dislocations (that are often composed of disclination pairs) and FCDs. We will review how the boundary conditions influence the behavior of these defects later in this review.

4.2 Dislocations.

Elementary topological defects in systems with broken translational symmetry are dislocations [1, 41, 42]. Dislocations are of two basic types, edge and screw, with the Burgers vector being perpendicular to the defect core in the first case and parallel to it in the second case. A typical edge dislocation in the cholesteric bulk is shown in Fig.4. By fitting the layers profile around

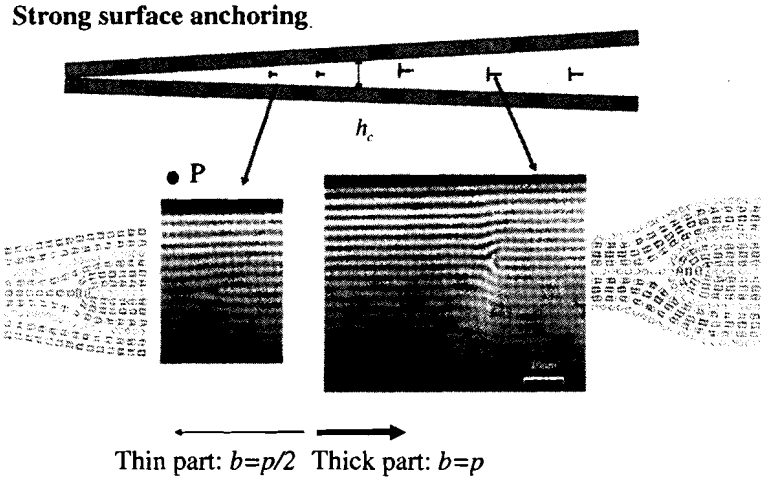

Figure 14. Dislocations with different Burgers vectors and different core structure in the thin and thick parts of the cholesteric wedge sample with strong polar anchoring energy, as seen by FCPM.

the line with the theoretical model [43], one can determine experimentally the penetration length $\lambda = \sqrt{K_1/B}$ which for cholesterics turns out to be ~$0.18p$ [44, 17].

Imagine that a lamellar phase is confined between two flat planes that are tilted with respect to each other by a small angle $\omega << 1$. If the layers are rigidly clamped by an appropriate substrate treatment to be parallel to the plates, and $\omega << 1$, the tilt results in a lattice of line defects-dislocations parallel to the edge of dihedron. Fig. 14 depicts different parts of the sample as imaged by FCPM technique. The edge dislocations in the thin part are always of the Burgers vector $b = p/2$, while the edge dislocations in the thick part are always of the Burgers vector $b = p$. The dislocations are split into pairs of disclinations: a line $b = p/2$ splits into τ and λ disclinations and a line $b = p$ splits into a $\lambda\lambda$ pair of disclinations. The nomenclature here, introduced by Kleman and Friedel [45], is based on the notation λ for the local director $\mathbf{n}$, χ for the direction of the helical axis, and $\tau = \lambda \times \chi$. In λ disclinations, the material λ director field is non-singular, while in τ disclinations, λ is singular and τ is not. Both types of lines are parallel to the cholesteric layers, except near the kinks, which change the level of the edge dislocations along the helicoid axis.

The core energy of dislocation is a significant portion of the total elastic energy. The energy in the far field (away from the core) in linear theory is [46]

$$F_{ff} = \frac{K_1 b^2}{4\pi\xi_x\lambda}\left[\exp(-2\beta) + \sqrt{\frac{\pi\beta}{2}}\,\mathrm{erf}\sqrt{2\beta}\right]. \tag{23}$$

where erf (...) is the error function, defined as $\mathrm{erf}\,(t) = \frac{2}{\sqrt{\pi}}\int_0^t \exp\,(-v^2)\,dv$, and $\beta = \frac{\xi_x^2}{4\lambda\xi_z}$; the two core sizes ξ_x and ξ_z are chosen along the two axes x and z, where the axis x is parallel to the extra later of the dislocation and perpendicular to the dislocation line. The two quantities ξ_x and ξ_z might be related in a non-trivial way, depending on λ and b. If one assumes $\xi_x^2 = 4\lambda\xi_z$, following the idea that perturbation of length δ_x along the layers propagates over the distance $\delta_z \tilde{} \delta_x^2/4\lambda$ along the z-axis, then $\beta = 1$, and

$$F_{ff} \approx 1.06\frac{Kb^2}{8\sqrt{2\pi\xi_z}\lambda^{3/2}} \approx 1.33\frac{Kb^2}{4\pi\xi_x\lambda} \approx \frac{Kb^2}{3\pi\xi_x\lambda}. \tag{24}$$

The function $F_{ff}\,(b)$, formally quadratic in Eq.(23), is in fact dependent on the model of the dislocation core. As suggested by Kleman [5], if the dislocation core is split into a pair of disclinations, then the horizontal cut-off ξ_x scales as b; roughly, $\xi_x \approx b/2$; at the same time ξ_z, being a distance along the z-axis, at which the semiwidth x of the parabola $x^2 = 4\lambda z$ reaches $p/2$, is taken as independent of b. With $\xi_x \approx b/2$, the far-field energy $F_{ff} \approx \frac{Kb^2}{3\pi\xi_x\lambda} \approx \frac{2Kb}{3\pi\lambda}$ is a linear function of b; the result implies that dislocations with large Burgers vector are stable against splitting into two or more dislocations with smaller b's.

The core energy of the split dislocations is estimated [5] as a sum $F_c\,(b) = F_{pair}\,(b) + F_c'$ of (I) the energy $F_{pair}\,(b)$ of a pair of disclinations separated by distance $2\xi_x \tilde{} b/2$; (II) core energy E_c' of the disclination lines themselves; this quantity depends little on b, but is extremely sensitive to whether the disclination is singular (large E_c') or not (small E_c'). As compared to the $\lambda^{-1/2}\lambda^{+1/2}$ pair, the core energy of the $\tau^{-1/2}\lambda^{+1/2}$ pair should contain an additional term $\tilde{} K\ln(p/r_c)$ that reflects the singular nature of $\tau^{-1/2}$ disclination with the core size r_c of the order of $1 \div 10$ molecular sizes [11].

For the $\tau^{-1/2}\lambda^{+1/2}$ pair, integrating the typical distortion energy density, $\frac{1}{2}\frac{K}{r^2}$, between $r = r_c$ and $r = b/2 = p/4$, one obtains

$$F_{c,\tau\lambda} = F_{pair} + F_c' \approx \frac{\pi}{2}K\ln(\frac{p}{4r_c}) + C_1 K, \tag{25}$$

where C_1 is a number of the order of unity. F_c' should not differ much from the estimate $F_c' = C_1 K = \frac{\pi}{8}K$ suggested by Oswald and Pieranski [4] for the singular core of a nematic disclination of winding number $\pm 1/2$, which implies

$C_1 = \pi/8 \approx 0.4$. For typical $p \approx 5$ μm and $r_c \approx 5$ nm, the logarithmic factor in Eq.(25) is relatively large, $\ln(\frac{p}{4r_c}) \approx 6$.

In the core of dislocation $b = p$ split into a $\lambda^{-1/2}\lambda^{+1/2}$ pair, the twist structure is distorted over the area $\tilde{}p^2$, and the core energy is roughly

$$F_{c,\lambda\lambda} = C_2 K, \tag{26}$$

where C_2 is another number of the order of unity. Therefore, one expects $F_{c,\lambda\lambda}$ to be about one order of magnitude smaller than $F_{c,\tau\lambda}$ when $p \approx 5$ μm and $r_c \approx 5$ nm. In other words, the $b = p/2$ dislocation has a much higher energy than the dislocation $b = p$ split into a $\lambda^{-1/2}\lambda^{+1/2}$ pair.

Why then $b = p/2$ dislocations with a very large core energy appear in the thin part of sample? Qualitatively, the reason is that inserting a slab of thickness $b = p/2$ into the wedge requires less compression energy as compared to a slab of thickness $b = p$. Obviously, the difference is significant only when the number N of layers in the wedge is small, and gradually decreases with an increase of N [46]. The balance of the core energy and the compression energy leads to a well-defined critical thickness h_c of the cholesteric wedge with a strong surface anchoring; for $h < h_c$, the dislocations are of the type $b = p/2$ with a singular core and at $h > h_c$, the dislocations are of the non-singular type with $b = p$.

The situation drastically changes when the boundary conditions at the plates are relaxed and the cholesteric axis can tilt away from the normal to the plates. Clearly, if the anchoring is sufficiently weak, the dislocation should escape from the system by going to the surface and disappearing there, Fig.4a,b,c. Fig.4a,b,c shows an edge dislocation confined between a plate with a strong anchoring at the bottom plate and a weak anchoring at the top plate. The Burgers vector is always $b = p$ and never $b = p/2$ in softly anchored wedges; the core is split into a $\lambda^{-1/2}\lambda^{+1/2}$ pair. The defects are very different from their $b = p$ counterparts in strongly anchored samples. Despite the fact that the $b = p$ dislocation by itself introduces a twist change by 2π, it always separates two Grandjean zones that differ only by one π rotation of $\mathbf{n}$. The fit is achieved by a surface desertion of one π twist at the boundary with weak anchoring, Fig.4c. The dislocation slowly glides towards the softly anchored plate, Fig.4b,c and coalesces with the deserted layer, producing a surface structure with a layer insertion, $2\pi - \pi = \pi$, Fig.4. Dislocations do not glide as straight lines: the motion involves formation and propagation of single kinks of height p, or pairs of kinks each of height $p/2$; the glide is hindered by a strong Peierls-Nabarro friction associated with the split core of the $b = p$ dislocations [46].

The existent theories [42] describe the surface-dislocation interaction in terms of the surface tension. Qualitatively, a dislocation creates a step at the boundary thus increasing the surface area and the surface energy. If this increase is smaller than the energy of elastic distortions around the dislocation in

bulk, the defect would be attracted to the surface. Although such an approach is definitely valid for many cases, including the free surfaces, generally, one also needs to consider the surface anchoring term. For a rigid boundary, the interaction is mediated by the anchoring effects: a dislocation approaching the boundary does not change the interfacial area but it does change the orientation of layers at the boundary.

Anchoring effects in cholesterics are difficult to describe analytically: near the substrate, the director field has to accommodate for both the elastic torques setting the helicoidal twist and surface interactions that keep $\mathbf{n}$ along a specific "easy axis" (or axes) that corresponds to the minimum of surface anchoring potential. Here we develop the coarse-grain model of Ch anchoring, by calculating the free energy per unit area of an interface, when the Ch "layers" make a small angle $\theta\,(z)$ with the substrate located at $z = 0$.

Under no external torque, the layers are parallel to the plate, as the polar surface anchoring keeps the director parallel to the surface. The azimuthal (in-plane) anchoring is vanishing. An external torque sets $\theta\,(z \to -\infty) = \theta_\infty$ far from the boundary. As the layers approach the boundary, surface anchoring modifies θ. If the surface anchoring is almost zero, then $\theta\,(z = 0)$ is close to θ_∞. If the surface anchoring is infinitely strong, then $\theta\,(z = 0) = 0$. The general case is considered below.

The free energy density of bulk deformations of a lamellar medium at scales much larger than the thickness of one lamella [1],

$$f = \frac{1}{2}K_1(div\mathbf{t})^2 + \frac{1}{2}K_3(\mathbf{t}\times curl\mathbf{t})^2 + \frac{1}{2}B(\frac{p-p_0}{p_0})^2, \qquad (27)$$

includes the curvature K-terms associated with the splay and bend of normal $\mathbf{t}$ to the layers and the B-contribution describing dilation/compressions of the layers. The splay constant K_1 and the Young modulus B are related to the Frank moduli of twist (K_{22}) and bend (K_{33}) of the director $\mathbf{n}$ by Lubensky-de Gennes relationships [47]: $K_1 = 3K_{33}/8$; $B = K_{22}(\frac{2\pi}{p_0})^2$. The bend (from the point of view of $\mathbf{t}$) constant K_3 can be derived from the Kats-Lebedev theory [48, 49]: according to E. I. Kats, $K_3 = \frac{K_{11}K_{33}}{2(K_{11}+K_{33})}$.

With $\mathbf{t} = (\sin\theta, 0, \cos\theta)$, the free energy per unit area of the boundary in the coarse-grained model of CLC is

$$W_{Ch} = \frac{1}{2}\int_{-\infty}^{0}\left[K_3\cos^2\theta(\frac{\partial\theta}{\partial z})^2 + B(\frac{\sin\theta}{\sin\theta_\infty} - 1)^2\right]dz + \frac{1}{4}W_p\sin^2\theta, \quad (28)$$

where the last term is calculated by assuming Rapini-Papoular anchoring potential for $\mathbf{n}$, $W_n = W_p n_z^2/2$, and then averaging over the in-plane director rotations. The contribution $K_1\sin^2\theta(\frac{\partial\theta}{\partial z})^2$ can be neglected for $\theta << 1$. Min-

imization of W_t yields the layers profile near the boundary,

$$t_x = \sin|\theta_\infty| \left[1 - \frac{W_p \sin|\theta_\infty|}{2\sqrt{K_3 B} + W_p \sin|\theta_\infty|} \exp \frac{-z}{\lambda_3 \sin|\theta_\infty|}\right] \qquad (29)$$

and the coarse-grained θ_∞-dependent anchoring potential for $\mathbf{t}$ that has an easy direction perpendicular to the bounding plate ($W_{Ch}(\theta_\infty = 0) = 0$):

$$W_{Ch}(\theta_\infty) = \frac{1}{2} \frac{W_p \sqrt{K_3 B} \sin^2 \theta_\infty}{2\sqrt{K_3 B} + W_p \sin|\theta_\infty|}. \qquad (30)$$

Depending on θ_∞ and the material parameters, $W_{Ch}(\theta_\infty)$ might be approximated by either $\sim \sin^2 \theta_\infty$ or $\sim \sin|\theta_\infty|$. The first form fits well to the experimental data on weak layer undulations [50], while the second one is better suited for large $|\theta_\infty|$ and W_p, when $W_{Ch}(\theta_\infty)$ is proportional to the number of layers crossing the boundary [51].

The interaction between the dislocation and the surface is determined by the free energy functional for the displacement field $u(x, z)$ of the cholesteric layers, written here in the linear approximation [42]:

$$F = \frac{1}{2} \int \left[K_1 (\frac{\partial^2 u}{\partial x^2})^2 + B(\frac{\partial u}{\partial z})^2\right] dz + W_{Ch}(\theta_\infty). \qquad (31)$$

If $W_{Ch}(\theta_\infty)$ were of the type $\sim \sin^2 \theta_\infty \sim \theta_\infty^2$, then all the results of the existing linear model [42] could have been applicable to our case, with simple replacements $\theta_\infty \to \gamma$ and $W_{Ch}(\theta_\infty) \to \sigma\gamma^2/2$, where σ is the surface tension coefficient at the free surface of the lamellar phase and γ is the tilt of the free surface. One of the results would be that for $\sigma > \sqrt{K_1 B}$, the interaction is repulsive and for $\sigma < \sqrt{K_1 B}$ it is attractive. However, Eq.(30) generally deviates from the simple $W_{Ch}(\theta_\infty) \sim \theta_\infty^2$ form and one has to resort to numerical analysis, using $\sqrt{K_3 B} = 10^{-5} J/m^2$, Fig.15. We compare the results to the "neutral" case (no interaction) in which $W_0(\theta_\infty) = \sqrt{K_1/B}\theta_\infty^2/2$ [42], see the line marked $\sigma = \sqrt{K_1 B}$ in Fig.15. For $W_p \sim 0.8 \times 10^{-4} J/m^2$, the curve $W_{Ch}(\theta_\infty)$ is below the curve $W_0(\theta_\infty)$; meaning that the interaction is attractive. In contrast, when $W_p \sim 4 \times 10^{-4} J/m^2$, the interaction is repulsive, as $W_{Ch}(\theta_\infty)$ runs above $W_0(\theta_\infty)$ for θ_∞ in the region of practical interest, $\theta_\infty < 0.4$, Fig.15 (note that the curves $W_{Ch}(\theta_\infty)$ and $W_0(\theta_\infty)$ might cross). The data are in good agreement with the experimental observations [17].

The consideration above of the dislocation lattices in the strongly anchored cholesteric samples is valid only for small dihedron angles, $\omega << 1$. What happens when ω increases? Initially, the density of dislocations increases linearly with ω ($\sim \omega$), but the process should stop at some critical angle, when the dislocations merge into one grain boundary. It turns out that in reality, proliferation of dislocations is interrupted by a lattice of FCDs. In the last section, we

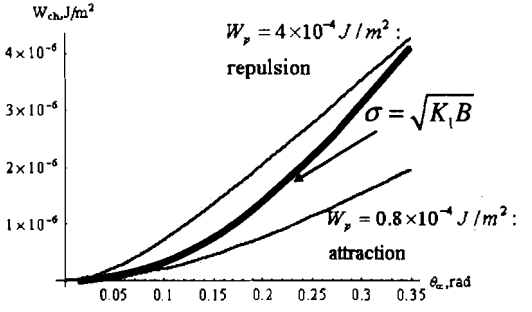

Figure 15. Cholesteric anchoring potential as a function of the angle of layer tilt to substrate for different polar anchoring coefficients W_p.

consider how the FCDs can relax boundary conditions in different geometries. We will deal with the smectic A phase; the director **n** is normal to the lamellae. The reason is that the FCDs are stable at scales of deformations larger than the interlamellar spacing and this spacing is much smaller in SmA (nanometers) than in Ch (micrometers).

4.3 Focal Conic Domains: Surface facetting and Grain boundaries

Textures of lamellar phases often show focal conic domains forming large families with an iterative fillings: smaller elliptical bases are embedded into the gaps between the larger ellipses. The first model of space filling with FCD has predicted that the iterative filling continues down to the smallest spatial scale possible, with the smallest FCD being of the size of penetration length λ. The result seems to be natural, as λ is the only characteristic length in a lamellar bulk, close to the thickness of one lamella. However, experimental onservations clearly show that the hierarchy of space filling has a macroscopic rather than microscopic cut-off, see e.g., Fig.16.

The physics of macroscopic residual regions can be explained most easily for a somewhat different case when the FCDs serve as the surface "facets" at the SmA-isotropic interface. Consider a large SmA droplet suspended in

Figure 16. Texture of focal conic domains formed by ellipse-hyperbola pairs (the elliptical bases are in the plane of observation and the hyperbolae are perpendicular to it). The smallest domain is clearly of macroscopic (tens of microns) rather than molecular (1 nanometer) size.

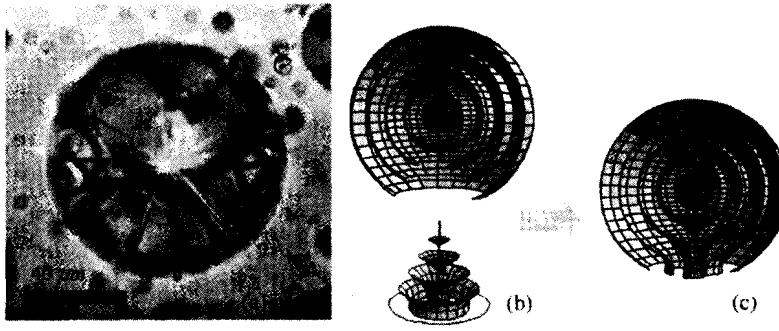

Figure 17. Toric focal conic domains serve as facets of the smectic A droplet suspended in an isotropic matrix that favors perpendicular orientation of smectic layers at the interface (a). The space filling scheme is illustrated in parts (b,c): a FCD is inserted instead of the spherically curved layers (b) to change the surface orientation of layers to perpendicular (c).

an isotropic matrix. If the matrix sets normal anchoring conditions for the director, then the equilibrium solution is clearly a concentric system of smectic layers with a radial hedgehog in **n**. Let the boundary conditions change to tangential, **n** being parallel to the interface (and the layers perpendicular to it). Experiments show that under tangential conditions, the droplet is filled with FCDs of degenerate (circle-straight line) type. The circular bases of the cones are located at the interface while the straight lines end at the center of the droplet, Fig.17a. The reason is that the molecules within the circular base are

parallel to the interface, thus reducing the surface anchoring energy, Fig.17b,c. However, one cannot cover the spherical surface of the sphere with a set of circles. The filling pattern is similar to Appolonian tiling: the gaps between the largest FCDs (of the size of the droplet radius) are filled with smaller circles, the remaining gaps are filled with yet smaller circles, etc. The pattern is fractal, although within a rather limited scale of lenthes with the maximum size being determined by the size of the sample and the smallest size being determined by the surface anchoring and bulk elasticity, as we shall see below.

Clearly, the iteration process stops when the elastic penalty of introducing the FCD becomes larger than the gain in the anchoring energy. The energy of a FCD of an arbitrary eccentricity has been calculated recently [1] to be

$$F_{FCD} = 4\pi a \left(1 - e^2\right) \mathcal{K}\left(e^2\right) \left[K_1 \ln \frac{2a\sqrt{1-e^2}}{r_c} - 2K_1 - \overline{K}\right] + F_c. \quad (32)$$

where $\mathcal{K}(x) = \int_0^1 \left[\left(1-t^2\right)\left(1-xt^2\right)\right]^{-1/2} dt$ is the complete elliptic integral of the first kind, e is the eccentricity of the ellipse. The core energy of the elliptical circular base can be assumed to be proportional to the perimeter of the ellipse $4a\mathcal{E}\left(e^2\right)$ (the core of the hyperbola softens out at distances of the order of the major axis of the ellipse away from the ellipse plane), $F_c = \alpha_1 4a\mathcal{E}\left(e^2\right) K_1$; here $\mathcal{E}(x) = \int_0^1 \left(1-t^2\right)^{-1/2} \left(1-xt^2\right)^{1/2} dt$ is the complete elliptic integral of the second kind; a is the major semiaxis of the ellipse; α_1 is a numerical coefficient of the order of 1. For a toric FCD,

$$F_{TFCD} = 2\pi^2 a \left[K_1 \ln \frac{2a}{r_c} - 2K_1 - \overline{K}\right] + F_{Tc} \quad (33)$$

with the core energy $F_{Tc} \approx \alpha_1 2\pi a K_1$. Comparing the estimates of the elastic energy $\tilde{} aK_1$ to the gain in surface anchoring energy $\tilde{} a^2\left(\sigma_{||} - \sigma_\perp\right)$ when the part of the spherical packing of layers, Fig.17, is replaced with the FCD, one obtains the radius, usually macroscopic, $a^* > \lambda$ of the smallest FCD in the iterative filling [52]:

$$a^* \tilde{} K_1 / \left(\sigma_\perp - \sigma_{||}\right) \quad (34)$$

where $\sigma_\perp$ and $\sigma_{||}$ are the surface anchoring energies for molecules perpendicular and parallel to the interface, respectively. In Fig.17a, the typical size of the smallest FCD is few microns.

Now we return to the problem of tilt grain boundary. Here, each FCD replaces a part of the grain boundary filled with dislocations. A rough estimate of the energy of dislocation-relaxed area of grain boundary is $\tilde{} \omega B \lambda a^2$; while

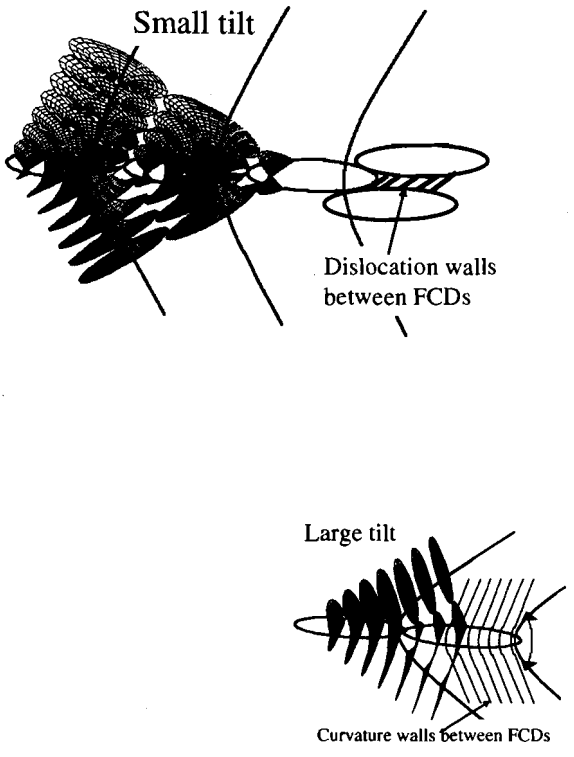

Figure 18. Two geometries of tilt grain boundary formed by an array of FCDs. For small angles, the residual regions between the FCDs are filled with dislocation lattices; for large angles, the resudial regions are filled with curvature walls.

the energy of the inserted FCD is $\tilde{}aK_1$. Therefore, large FCDs will fill in the grain boundary, then smaller FCDs will fill the gaps between them, and so on, until the FCD bases becomes as small as

$$a^* \tilde{} \lambda/\omega; \tag{35}$$

the remaining residual areas between the FCDs will preserve the structure of dislocation grain boundary. The residual areas can be very large, $a^* >> \lambda$, when the angle ω is small; for more detailed calculations, that take into account the particular scaling behavior of the FCD hierarchy, see [53]. Note also that when ω becomes larger than approximately $\pi/2$, then the dislocations in the residual areas are replaced by curvature walls. Figure 18 illustrate the two geometries for tilt grain boundaries.

5. Summary

We discussed topological and elastic properties of various topological defects in liquid crystals and demonstrated that the restrictions imposed by bounding surfaces are of prime importance for the stability of the defects. For example, a nematic droplet emerging from the isotropic phase might contain stable topological defects when it becomes larger than some critical size determined by the surface anchoring and elastic constants. An edge dislocation in a 1D lamellar phase (cholesteric, smectic) might be repelled from the surface or attracted to it depending on the strength of surface anchoring that imposes some well-defined director orientation at the surface. Although many aspects of defects in liquid crystals are well understood, there is still a number of important problems to explore. One of the most important is that of defect dynamics which we did not discuss here. New experimental techniques, such as the fluorescence confocal polarizing microscopy, are expected to expand significantly our understanding of defects in soft matter.

Acknowledgments

The work was partially supported by the donors of the Petroleum Research Fund, grant 35306-AC7. I thank T.W.B. Kibble and H. Arodz for the opportunity to present this review at the NATO ASI&COSLAB School "Pattern of Symmetry Breaking" in Cracow.

References

[1] Kleman, M. and Lavrentovich, O.D. (2003) *Soft Matter Physics: An Introduction.* Springer-Verlag, New York.

[2] de Gennes, P.G., and Prost, J. *The Physics of Liquid Crystals* (Clarendon Press, Oxford, 1993).

[3] Chaikin, P.M. and Lubensky, T. (1995) *Principles of Condensed Matter Physics.* Cambridge University Press, Cambridge.

[4] Pieranski, P.and Oswald, P. (2000) *Les Cristaux Liquides, Tomes 1 et 2.* Gordon and Breach Science Publishers, Paris.

[5] Kleman, M. (1983) *Points, Lines and Walls in Liquid Crystals, Magnetic Systems and Various Ordered Media.* Wiley, Chichester.

[6] Kurik, M.V. and Lavrentovich, O.D. (1988) *Usp. Fiz. Nauk,* **154**, *381-431 [Sov.Phys.Usp.* **31**, *196-224]*

[7] Faetti, S., and Palleschi, V. (1984) Phys. Rev. A 30, 3241-3251.

[8] Bradshaw, M.J, Raynes, E.P., Bunning, J.D., and Faber, T.E. (1985) J. Physique 46, 1513-1520.

[9] Bowick, M.J., Chandar, L., Schiff, E.A., and Srivastava, A.M. (1994) Science 263, 943-945.

[10] Chuang, I., Durrer, R., Turok, N., and Yurke, B. (1991) Science 251, 1336-1342. Yokoyama : Yokoyama, H. (1988) J. Chem. Soc. Faraday Trans. 2, 84, 1023.

[11] Lavrentovich, O.D. and Kleman, M. (2001), Ch.5: Cholesteric Liquid Crystals: Defects and Topology, in: *Chirality in Liquid Crystals*, Bahr, C. and Kitzerow, H. (eds.), Springer-Verlag, New York.

[12] Lavrentovich, O.D., Pasini, P., Zannoni, C., and Žumer, S. (editors) (2001) *Defects in Liquid Crystals: Computer Simulations, Theory and Experiments.* Kluwer Academic Publishers, the Netherlands.

[13] Hartshorn, N.H. (1974) *The Microscopy of Liquid Crystals.* Microscope Publications, London.

[14] Smalyukh, I.I., Shiyanovskii, S.V. and Lavrentovich, O.D. (2001) *Chem. Phys. Lett.*, **336**, 88-96.

[15] Shiyanovskii, S.V., Smalyukh, I.I., and Lavrentovich, O.D. (2001), see Ref.[12], p. 229-270.

[16] See, e.g., R.H. Webb, *Rep. Prog. Phys.* **59**, 427 (1996); W.T. Mason, (ed.) (1999) *Fluorescent and Luminescent Probes for Biological Activity: a Practical Guide to Technology for Quantitative Real Time Analysis.* Calif.:Academic Press, San Diego; Pawley, J.B. (ed.) (1995) *Handbook of Biological Confocal Microscopy.* Plenum Press, New York.

[17] Smalyukh, I.I., and Lavrentovich, O.D. (2003) *Phys. Rev. Lett.*, **90**, 085503

[18] Toulouse, G. and Kleman, M. (1976) *J. Phys. lett. (Paris)* **37**, L-149-151; Kleman, M. (1977) *J. Phys. Lett. (Paris)* **38**, L-199; Kleman M. and Michel L. (1978) *Phys. Rev. Lett.* **40**, 1387.

[19] Volovik, G.E. and Mineev, V.P. (1976) *Pis'ma Zh. Eksp. Teor. Fiz.* **24**, 605 [*JETP Lett.* **24**, 595]; (1977) *Zh. Eksper. Teor. Fiz.* **72**, 2256-2274 [*Sov. Phys. JETP* **45**, 1186-1196].

[20] Volovik, G.E. (1978) *Pis'ma Zh. Eksp. Teor. Fiz (USSR)* **28**, 65-67 [*JETP Lett. (USA)* **28**, 59-61].

[21] Volovik, G.E. and Lavrentovich, O.D. (1983) *Zh. Eksper. Teor. Fiz.(USSR)* **85**, 1997 (1983) [*Sov.Phys.JETP (USA)* **58**, 1159 (1983)]

[22] Toulouse, G. (1977) *J. Phys. Lett. (Paris)* **3**, L-67 - L-68.

[23] Chiccoli, C., Feruli, I., Lavrentovich, O.D., Pasini, P., Shiyanovskii, S.V., Zannoni, C. (2002) *Phys. Rev. E* 66, 030701R.

[24] Madhusudana, N.V. and Pratibha, R. (1983) *Mol. Cryst.Liq.Cryst.* **103**, 31-47.

[25] Lavrentovich, O.D. and Nastishin, Yu.A. (1990) *Europhys. Lett.* **12**, 135-141.

[26] Frank, F.C. (1958) On the theory of liquid crystals, *Disc. Faraday Soc.* **25**, 19-28.

[27] Anisimov S.I. and Dzyaloshinskii, I.E. (1972) *Zh. Eksp. Teor. Fiz.* **63**, 1460-1471 [*Sov. Phys. JETP* **36**, 774-783].

[28] Cladis, P.E. and Kleman M. (1972) *J. Physique (Paris)* **33**, 591.

[29] Meyer, R.B. (1973) *Phil. Mag.* **27**, 405-424.

[30] Mori, H. and Nakanishi, H. (1988) *J. Phys. Soc. Japan* **57**, 1281.

[31] Lavrentovich, O.D., Ishikawa T., and Terentjev, E.M. (1997) *Mol. Cryst. Liq. Cryst.* **299**, 301.

[32] Ishikawa, T. and Lavrentovich, O.D. (1998) *Europhys. Lett.* **41**, 171-176.

[33] Lavrentovich, O.D. (1992) *Phys. Rev. A* **46**, R722-725.

[34] Lavrentovich, O.D. (1998) *Liq. Cryst.* **24**, 117-125.

[35] Poulin, P. Stark, H., Lubensky, T.C., and Weitz, D.A. (1997) *Science* **275**, 1770-1773.

[36] Nastishin, Yu.A., Polak, R.D., Shiyanovskii, S.V., Bodnar, V.H. and Lavrentovich, O.D. (1999) *J. Appl. Phys.* **86**, 4199.

[37] Rapini, A. and Papoular, M. (1969) *J. Phys. (Paris) Colloq.* **30**, C-4.

[38] Shiyanovskii, S.V., Glushchenko, A., Reznikov, Yu., Lavrentovich, O.D. and West, J.L.(2000) *Phys. Rev. E*, **62**, R1477.

[39] Kurik, M.V., and Lavrentovich, O.D. (1983) *Zh. Eksp. Teor. Fiz.* **85**, 511-526 [*Sov.Phys. JETP* **58**, 299-307]

[40] Yokoyama, H. (1988) *J. Chem. Soc. Faraday Trans.* **2**, 84, 1023.

[41] Pershan, P.S. (1974) *J. Appl. Phys.* **45**, 1590.

[42] Holyst, R. and Oswald, P. (1995) *Int. J. Mod. Phys.* B **9**, 1515.

[43] Brener, E. A. and Marchenko, V. I. (1999) *Phys. Rev. E* **59**, R4752.

[44] Ishikawa, T., and Lavrentovich, O.D. (1999) *Phys. Rev. E* **60**, R5037.

[45] Kleman, M., and Friedel, J. (1969) *J. Physique Colloq.* **30**, C4-43.

[46] Smalyukh, I.I., and Lavrentovich, O.D., (2002) *Phys. Rev. E* **66**, 051703.

[47] Lubensky, T. C. (1972) Phys. Rev. A **6**, 452.

[48] E.I. Kats and V.V. Lebedev, *Fluctuational Effects in the Dynamics of Liquid Crystals*, (Springer-Verlag, New York, 1994), Chapter 5, p.170.

[49] The result is obtained by collecting the terms with $(\mathbf{t} \times curl\mathbf{t})^2$, $(div\mathbf{t})^2$, etc., and neglecting the divergence (surface-like) terms in Eqs. (5.1.27, 33) of Ref.[48].

[50] Ishikawa, T. and Lavrentovich, O.D. (2001) *Phys. Rev. E* **63**, R030501.

[51] Lavrentovich, O.D. and Yang, D.-K. (1998) *Phys. Rev. E* **57**, R6269.

[52] Lavrentovich, O.D. (1986) *Zh. Eksp. Teor. Fiz.* **91**, 1666-1676 [*Sov.Phys. JETP* **64**, 984-990]

[53] Kleman, M. and Lavrentovich, O.D. (2000) *Eur. Phys. J E* **2**, 47-57.